Materials & Design 244 (2024) 113098

Contents lists available at ScienceDirect

Materials & Design

journal homepage: www.elsevier.com/locate/matdes

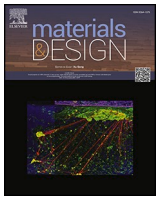

Twinning-inspired hexagonal close-packed metamaterials for enhanced energy absorption

Giovanni Zappa [a], Lorenzo Cocchi [a], Sara Candidori [b], Federica Buccino [b,c], Laura Vergani [b,c], Serena Graziosi [b,*]

[a] Politecnico di Milano, School of Industrial and Information Engineering, Piazza Leonardo da Vinci 32, 20133, Milan, Italy
[b] Politecnico di Milano, Department of Mechanical Engineering, Via la Masa 1, 20156, Milan, Italy
[c] IRCCS Orthopedic Institute Galeazzi, Milan, Italy

ARTICLE INFO

Keywords:
Architected materials
Metamaterials
Hexagonal close-packed
Crystal twinning
Additive manufacturing

ABSTRACT

Additive Manufacturing provides unprecedented opportunities for designing and producing intricate, architected materials with exceptional properties while maintaining reduced weight. One of the most straightforward ways to create such structures is to mimic the lattice geometries of crystals. New approaches are now exploring how to influence the behaviour of these structures by mimicking not only the crystal arrangement but also peculiar mechanisms occurring at the crystallographic scale. In such a context, this study first presents a hexagonal close-packed (HCP) lattice derived from the homonymous crystal structures of Ti or Zr metals. Subsequently, the twinning phenomenon responsible for the plastic deformation of these metals is reproduced geometrically into this structure to improve its energy absorption capability. Compressive tests conducted on 3D-printed samples confirm such a hypothesis: the specific energy absorption of twinned structures is significantly higher than that of the equivalent HCP ones, with an increase of up to 24.3%. Introducing twinned regions stabilises the plastic deformation despite a limited reduction of the peak stress. Therefore, replicating the twinning metallurgical mechanism within an HCP-inspired metamaterial proves successful, further validating the approach of mimicking and transferring atomic phenomena at a different scale to tailor the properties of architected materials.

1. Introduction

The rapid development of Additive Manufacturing (AM) is unlocking new possibilities in designing and fabricating complex architected materials (or mechanical metamaterial [1]), offering enhanced mechanical properties and structural performance at a reduced weight [2,3]. Among the different types of non-stochastic architected materials are those formed by a periodic arrangement of unit cells consisting of a regular network of struts [4,5], also known as strut-and-node [6] or truss [7] lattices. Extensive and comprehensive studies have been carried out with a focus on their elastic and plastic deformations [7], toughness, and energy absorption [7] properties, analysing the influence of various parameters. Intuitively, among the determinants of their behaviour is the topology of the unit cell [4]. Maxwell's stability criterion can be applied to distinguish bending- and stretching-dominated structures depending on the nodal connectivity [4,8]. However, studies have also demonstrated the dependency of such a classification on other aspects. For example, the Octet lattice, classified as stretching-dominated, can be used for energy absorption applications at moderately high relative densities [7]. The loading direction also influences such behaviour [9]. Alterations in the lattice unit cell geometry also modify the deformation behaviour, such as the introduction of additional vertical beams [10], tactical structural modifications [11], the change of the beams' slenderness ratio [7,12] or of their shape (e.g., tapered [7,13], hollow [14], semi-circular [15] or squared [16] vs. circular cross-sections). The mechanical response of a structure is also influenced by the number of repetitions of unit cells; the elimination of such dependence is found to be 5 in all directions, but also decreasing to 4, the results are acceptable [17]. In addition to geometric factors, the base material [18–21] and the potential presence of manufacturing defects [22,23] dramatically influence the mechanical response.

Another point to underline is that the design of these strut-based lattices has been strongly inspired by Bravais lattices [24,25] and crystallographic symmetries [26], with the atoms' position and atomic

* Corresponding author.
E-mail address: serena.graziosi@polimi.it (S. Graziosi).

https://doi.org/10.1016/j.matdes.2024.113098
Received 6 February 2024; Received in revised form 16 May 2024; Accepted 16 June 2024
Available online 23 June 2024

bonds reproduced by nodes and beams, respectively [20,27]. Among the seven crystalline systems, the cubic one is the most commonly used, as it includes the three famous simple cubic (SC), face-centred cubic (FCC) and body-centred cubic (BCC) unit cells [27]. However, other systems could also be considered, although the repetition of the basic unit along the three directions may not be as trivial as in the case of highly symmetric cells. For example, Bian and colleagues [28] attempted to fill this gap by designing new lattice structures that mimic triclinic (TC) crystal materials. In addition, tetragonal- and orthorhombic-inspired metamaterial lattices can be easily created by stretching a cubic lattice along one or two of its main directions, respectively. Such unit cells can be obtained by considering a prismatic bounding box with a square (for the tetragonal) or rectangular (for the orthorhombic) base. The repetition of a single unit cell forms a homogeneous lattice, which resembles the single crystals in the collapse of mechanical strength after yielding [20]. The formation of shear bands found in homogeneous architected materials (related to the plastic yield, bending or buckling of constituent struts [4]) is indeed similar to the dislocation movements found in single crystals, which are responsible for their plastic flow [20,29]. This similarity inspires a transformative approach to designing innovative architected materials with high strength and damage-tolerant behaviour [20]. Such an approach is based on the mimicry of the crystallographic microstructure and the integration of associated hardening mechanisms at the macro- or mesoscale [20].

The concept of metallurgical-inspired metamaterials was first proved by designing structures resembling polycrystals with multiple domains, referred to as grains, characterised by the same unit cell type but with different orientations [20,29]. It was shown that the increase of the yield strength with the reduction of meta-grain size in metamaterials follows the well-known metallurgical Hall-Petch relationship [30–32], and it is due to the effectiveness of *meta*-grain boundaries in stopping shear band propagation [20,29]. Moreover, as boundary coherency influences the strengthening effect in polycrystals [33] similarly, strut connectivity at the boundary controls the hardening effect [29]. Besides, in the case of heterogeneous lattices made of different unit cells, innovative strategies using transition cells were also developed to combine unit cells with different nodal connectivity, taking inspiration from the connections observed in the grain boundaries of polycrystalline materials [34].

Other hardening effects can be successfully translated to architected materials, such as precipitation [20,35] and multi-phase hardening [20]. The former consists of particle dispersion inside the metallic matrix, which restricts dislocation movement [36]. Similarly, including harder domains in a softer architected material alters shear band propagation, strengthening the overall architected material [20]. More interestingly, the applicability of Orowan's law, which states the inverse proportionality between additional strength and precipitate spacing [37,38], to architected materials was recently proven [35]. Finally, multi-phase hardening was successfully imitated by assigning different lattice types to different macro-lattice domains [20]. Additionally, multi-phase mimicry of lamellar structures, as those found in TiAl alloys, can be effectively used to finely control the mechanical response of metamaterials, providing a programmable and multi-stepped response [35]. Architected material behaviour is also affected by the base material's choice [20,39]. Using a crystalline material to fabricate crystal-like structures generates a hierarchical multiscale structure, called metacrystal, in which synergistic effects contribute to strengthening [20,32,40]. The reproduction of the crystal twinning mechanism was also employed for lattice material generation, designing structures featuring a specular geometry with respect to a twinning plane (TP). Such a mechanism represents a particular planar defect which occurs when the atoms at the two sides of the plane are arranged as if mirrored with respect to it [41]. This condition represents an interesting mechanism for improving the material's mechanical behaviour. In metamaterials, TPs act as shear band stoppers and produce a symmetrical distribution of them [28,42–44].

This concept of twinning boundaries is already inspiring relevant studies in the field of architected materials. For example, it was introduced in the triply periodic minimal surface (TPMS) lattice design to effectively control the deformation behaviour and avoid catastrophic failure [43]. Wu et al. [44] found that incorporating twin boundaries in stretching-dominated truss lattices improves crack-propagation resistance and energy absorption efficiency. The validity of the Hell-Petch effect was also demonstrated for twinning metamaterials [28,44]. Twin boundaries were also introduced in the TC lattice designed by Bian et al. [28], proving effective in enhancing energy absorption performance. Lastly, Song and colleagues [42] designed new truss-based lattices with horizontal and vertical twinning boundaries, demonstrating the possibility of tailoring the mechanical properties by controlling the number of twinning boundaries.

This study falls into this context of metamaterial design and proposes an innovative approach to exploit the twinning phenomenon. First, it presents a hexagonal close-packed (HCP) lattice inspired by the homonymous crystal structure. Then, a twinned region is introduced inside this HCP lattice to improve energy absorption without significantly reducing stiffness and strength. Indeed, the compression behaviour of ductile HCP metals, such as titanium and zirconium, demonstrates that their deformation is accommodated by this twinning phenomenon [45,46]. This study is, therefore, based on the hypothesis that introducing a twinned region inside a structure is expected to promote a more controlled deformation behaviour. Another contribution of this study is that although HCP, together with BCC and FCC, is the lattice forming 90% of metallic materials, few examples of HCP-inspired lattices can be found in the literature. Only recently, an HCP unit cell was presented in the work of Liu and Pham [35], where it was exploited in the design of the previously mentioned lamellar structure inspired by TiAl alloys. Another example of an "HCP-like lattice" can be found in [47], although the authors refer to it as an Octet truss lattice. The same authors analysed its mechanical behaviour through tensile [47], compressive [48], fracture [47,49], and fatigue analyses [50–53]. However, the compressive behaviour was only characterised by specimens fabricated in a brittle resin as base material [48]. In addition, in that study, the unit cell presents several interrupted beams that were not removed when the lattice had been created, thus generating a different overall beam arrangement compared to the HCP described in this study.

Hence, this work follows the innovative approach of mimicking metallurgical phenomena at a larger scale to design new architected materials. Although other studies already proposed twinning-inspired lattices, the mimicry strategy implemented in the present work is novel. While those studies [28,42–44] applied the twinning by mirroring their unit cell along specific planes, creating a layered architecture, here that mechanism is replicated as faithfully as possible as it occurs in HCP ductile metals. The intent is to explore whether introducing this phenomenon would affect the mechanical behaviour of HCP metamaterials similarly to that occurring at the microscale to improve their energy absorption performance. Specifically, this study starts by experimentally comparing the compressive behaviour of the HCP lattice with that of a standard Octet. Then, once the superior compressive capabilities of the HCP are demonstrated, the twinning phenomenon is implemented, and its positive influence is proved.

The rest of the paper is structured as follows: Section 2 gives the main metallurgical notions concerning HCP and FCC cells and their deformation mechanisms, which are necessary to understand the design methodology described later; Section 3 details the material and methods employed with a particular focus on the design approach developed to implement the twinning mechanism and the experimental tests performed; Section 4 details and comments on the experimental results; Section 5 ends the paper.

2. Deformation mechanisms of HCP and FCC structures

One of the key properties of crystal lattices is the "packing density", i.e., the fraction of the volume filled by atoms considered rigid spheres.

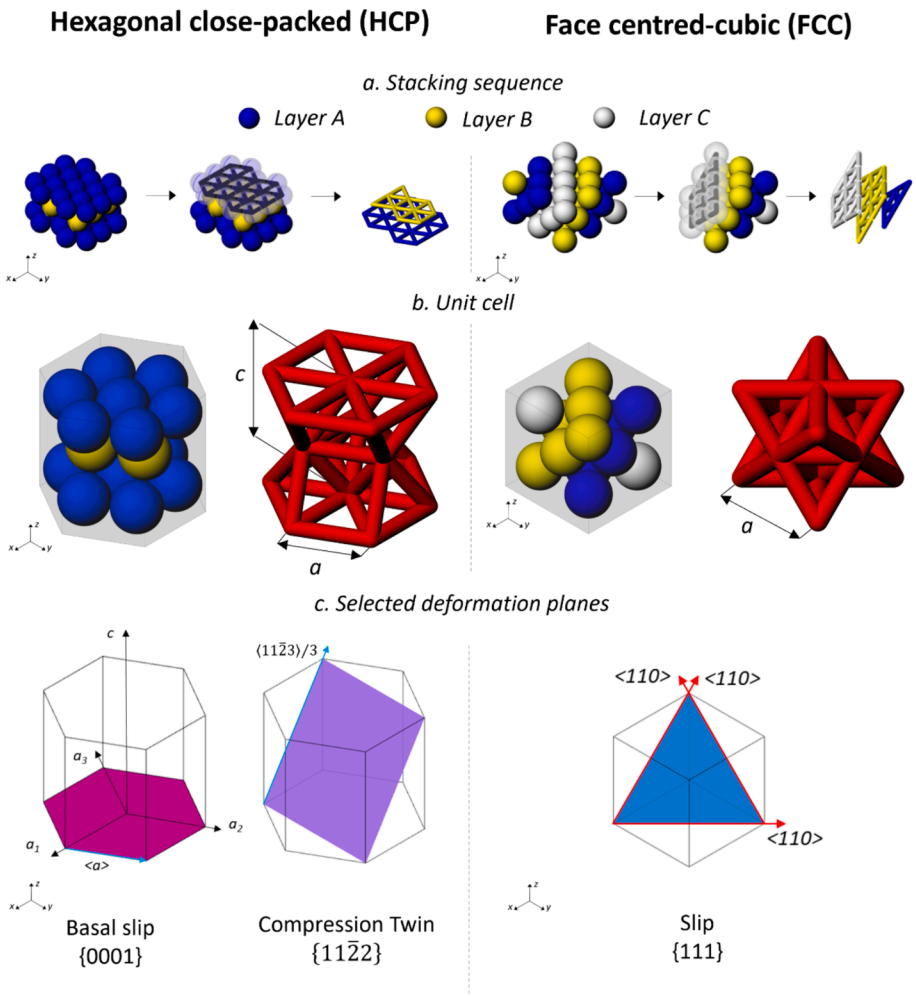

Fig. 1. Comparison between HCP and FCC structures. a) Stacking sequence: HCP and FCC lattices are obtained by stacking rigid spheres of equal diameter following an "ABABAB…" or "ABCABC…" sequence, respectively. b) Single unit cell: HCP and Octet unit cells with their geometrical parameters. c) Selected deformation modes: slip usually occurs along the close-packing directions (basal slip $<$ a $>$ in the HCP and $\langle 1\,1\,0\rangle$ slip in the FCC). Under compression along the c-axis, HCP cells can accommodate deformation by twinning. Slip/twin planes are highlighted with colours, while Burger vectors are shown by light blue (for the HCP) and red (for the FCC) arrows. All representations are shown as isometric views. Fig. 1 c is inspired by [54]. (For interpretation of the references to colour in this figure legend, the reader is referred to the web version of this article.)

The HCP structure is so called because it is one of the two ways rigid spheres can be packed together in space with the highest possible density and still have a periodic arrangement [54]. The HCP cell in this study is compared with the Octet. The Octet is an FCC-inspired unit cell [55,56] and, like the HCP, is the lattice with the highest packing density possible, equal to $\frac{\pi}{3\sqrt{2}} \approx 0.74$. Given such a characteristic, both structures have the same nodal connectivity, equal to 12 [57]. Although the similarities between the two crystals are not visible at first sight, they can be caught by considering how they can be obtained by stacking rigid spheres of the same size. As shown in Fig. 1 a and b, both lattices are built through the repetition of layers of atoms arranged at the vertices of a triangular grid; the only difference comes from the stacking sequence of the layers: the HCP follows a stacking sequence of "ABABAB…" layers, while the FCC follows an "ABCABC…" sequence [54] (stacking sequence in Fig. 1 a).

Despite this, the dissimilarity in the stacking sequence leads to significant differences in their deformation mechanisms, with those of HCP metals being more complex than FCC ones [45] due to several factors. In addition to the lower symmetry, HCP metals differ in their crystallographic structure. The c/a axial ratio (where c and a are the total height and the length of the hexagon edge, respectively; see Fig. 1 b) varies from one metal to the other.

As known from the literature [45], the ideal c/a value (i.e., the one guaranteeing the maximum sphere packing) is $\sqrt{8/3} \approx 1.63$. However, HCP metals can have values ranging from 1.58 for Beryllium up to 1.89 for Cadmium. This steric effect is an important aspect that prevents the HCP metals from being considered a homogenous class of metals [45], contributing to their highly different mechanical behaviour.

In general, the dislocation movement is the primary mechanism responsible for the plastic deformation of metals; it occurs mainly along the lattice close-packed direction on the close-packed planes. Slips in FCC crystals occur along the previously mentioned close-packed planes (Fig. 1 c). Specifically, the slip plane is of type $\{1\,1\,1\}$, and the direction is of type $\langle 1\,1\,0\rangle$. Given the permutations of the slip planes and directions, FCC has 12 slip systems [45,58]. Slips in HCP metals are much more limited; because of this, the twinning mechanism competes with the slip in plastic deformation and can play an influential role [45,59].

Among the possible slip planes of HCP metals, basal slip (i.e., the dislocation movement on the base plane of the HCP cell shown in Fig. 1 c) is the most common [60]. The activation of a specific deformation mechanism in HCP is governed by the c/a axial ratio and by the orientation of the lattice with respect to the load. An interesting aspect relevant to this study is the case of a compression or tension load along the z-axis (see Fig. 1 for the reference system). For geometrical reasons,

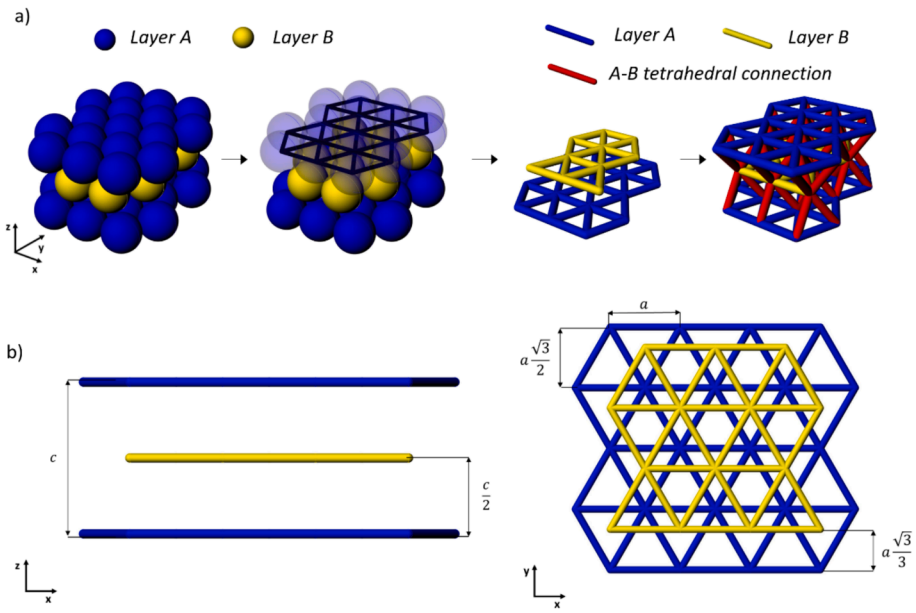

Fig. 2. Generation of an HCP structure and its parametrisation. a) ABA sequence of stacked atoms forming the HCP crystal; substitution of each layer with a triangular grid and connection of two adjacent grids through tetrahedral beams (from left to right); b) parametrisation of the HCP lattice.

the basal slip (Fig. 1 c) cannot accommodate axial loads aligned along the z-axis [45,61]. So, many studies were conducted to understand the underlying mechanism that accommodates the deformation in this situation. Beryllium is reported to assume a brittle failure [46]; zinc undergoes much greater plastic strain in tension due to the accommodation of $\{10\bar{1}2\}$ twinning [46], while titanium accommodates the strain almost entirely by $\{11\bar{2}2\}$ compression twins [61]. In Magnesium [60,62], twins can occur along the $\{10\bar{1}1\}$ and $\{11\bar{2}2\}$ compression planes. Zirconium [45] deforms by $\{11\bar{2}2\}$ twinning and, at elevated temperatures, by $\{10\bar{1}2\}$ and $\{10\bar{1}1\}$ twins. It is, therefore, evident how the twinning plays a fundamental role in the deformability of HCP metals.

3. Materials and methods

3.1. Sample design

The digital models of the HCP and HCP-twinned structures were created in the *Grasshopper* environment of *Rhinoceros 7*. For the Octet, the *Intralattice* plugin was employed [63]. Details about the HCP and HCP-twinned structures beam and node arrangements are provided below. Besides, how the tuning of the structure geometric parameters has been performed to guarantee the sample printability and

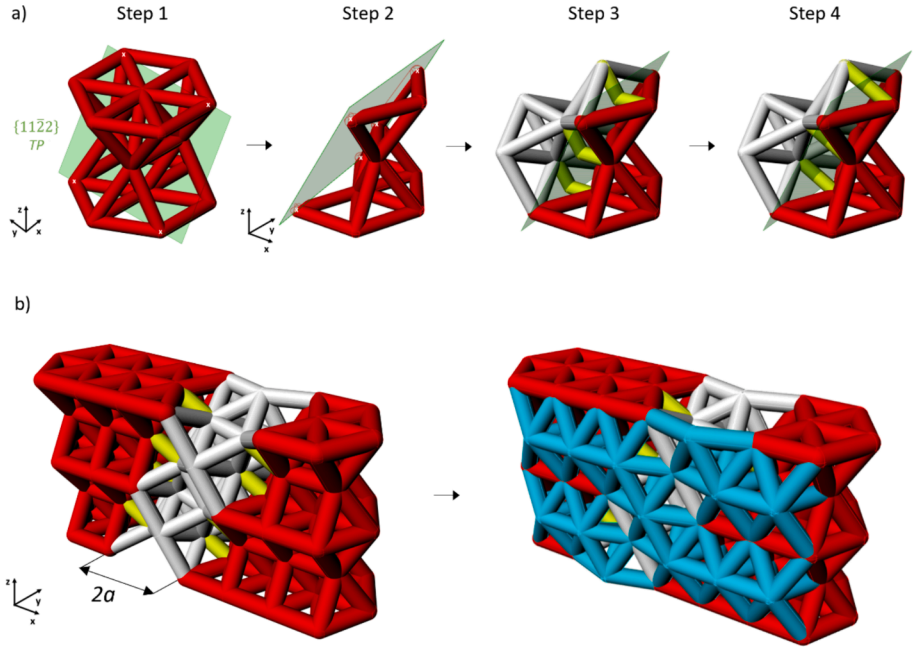

Fig. 3. Design of the twinned HCP structure (TwHCP). a) Mirroring of the HCP unit cell with respect to the $\{11\ \bar{2}2\}$ plane and beam adjustments (TP stands for "Twinning Plane"); b) introduction of the twinned region (in grey) inside an HCP lattice and new beam insertion (they are light-blue coloured) to guarantee nodal connectivity. (For interpretation of the references to colour in this figure legend, the reader is referred to the web version of this article.)

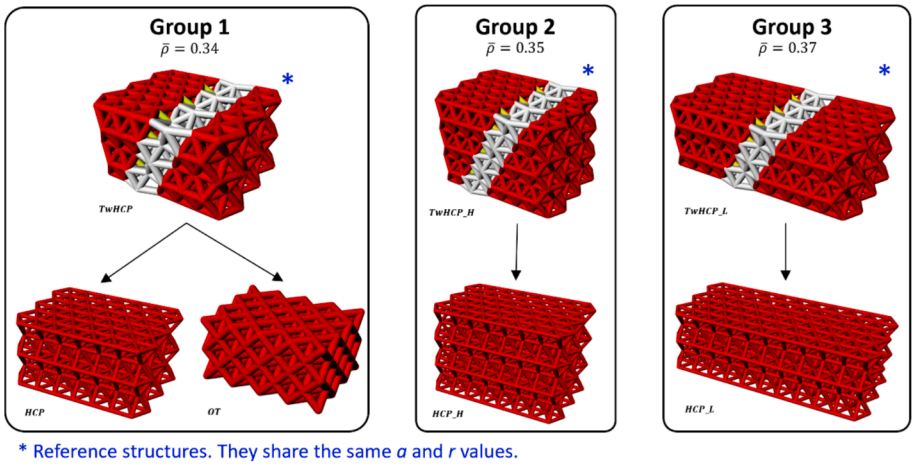

Fig. 4. Relationships between the seven lattice structures analysed in this work. These can be divided into three groups. In each group, the twinned structure was taken as a reference, and one or two equivalent (=same $\bar{\rho}$) structures were developed. The letters "a" and "r" indicate the beams' length and radius, respectively, and are shared by the different twinned lattices. "OT" stands for Octet, "HCP" for the Hexagonal Closed package, and "TwHCP" for the twinned variant of the HCP. The remaining labels indicate further variants of the "HCP" and the "TwHCP". Specifically, "_H" and "_L" are added to indicate the propagation of the twinning phenomenon along the structure height or length, respectively.

comparability is also clarified. Seven types of structures were tested, classified into three groups.

3.1.1. The HCP structure

Given its intricate nature, the HCP structure was not created by reproducing a single unit cell but by replicating the crystal lattice. The HCP lattices are built by alternating two layers of closed-packed atoms, arranged at the vertices of a triangular tilting, stacked in an ABA sequence (Fig. 2 a, left) [54]. Assuming the atoms are the lattice's nodes, their connection creates two triangular grids corresponding to the A and B layers (blue and yellow in Fig. 2 a, right). The connection between the A and B layers is achieved through vertical beams connecting the corners of the A-layer triangles to those of the B-layer triangles, which lie exactly on the projection of their centre in the B-layer plane (red beams in Fig. 2 a, right). This produces an ordered array of tetrahedrons. The design was parametrised to depend only on the imposed length of the beam (a). The two triangular grids are shifted of $a\frac{\sqrt{3}}{3}$ in the y-direction and equally spaced of c/2 in the z-direction (Fig. 2 b). As already explained, a is the edge of the triangles, while c is the height of the HCP unit cell (Fig. 1).

3.1.2. The twinned HCP (TwHCP) structure

For the development of the twinned region, a specific twinning plane, i.e., $\{11\bar{2}2\}$, was selected from the possible twinning systems of HCP metals (Fig. 1 c and Fig. 3 a, step 1). It allows a straightforward design as it is the only twinning plane intersecting at least one node in all A and B layers (Fig. 2 and Fig. 3 a, step 2). Therefore, this guarantees connectivity between the twinned and HCP regions. To build the twinned region first, the portion of the HCP cell above the TP was removed (Fig. 3 a, step 2), and a mirroring of the remaining beams/nodes was then performed with respect to the TP (Fig. 3 a, step 3). Some adjustments were made to ensure all beams within the cell have a linear geometry (Fig. 3 a, steps from 3 to 4). In particular, the beams intersected (and therefore cut) by the plane were removed and replaced by new ones that connect the mirrored and non-mirrored nodes linearly (yellow beams in Fig. 3 a). Far from the mirroring interface, both the unperturbed and the twinned regions evolve according to the classical HCP lattice geometry (Fig. 3 b). A specific $(c/a) = \sqrt{3}$ was chosen to ensure that specific vertical beams would become parallel to the x-y plane after mirroring. This choice was made to simplify the printing process since the expansion of the twinned region would require the presence of parallel beams in contact with the printing plate. The final structure was obtained through a series of steps, including developing the twinned part within a defined spatial region, laterally bounded by the twinning plane and a parallel plane, whose length is $2a$ in the x-direction (Fig. 3 b, left). The twinned section was then subjected to a second mirroring process along a second twinning plane, which restored the original HCP lattice geometry at the other interface. A second row of triangles was added to the B layer (light blue beams in Fig. 3 b, right) to improve node connectivity within the twinned section.

3.1.3. Relative density calculation and sample classification

To compute $\bar{\rho}$ (i.e., the structure's relative density), the volume of the structure was analytically calculated. A dedicated algorithm was developed in Matlab® since the HCP (Fig. 2) and the TwHCP (Fig. 3) lattices do not feature a standard periodic repetition of the unit cell along the reference axes. The analytical approach implemented in Matlab is described in detail in the **Supplementary Material** (see **Supplementary Material A**. Volume and relative density computation), where the various approaches for replicating the HCP and its twinned versions are explained. Besides, a second analytical Matlab model was developed to calculate the $\bar{\rho}$ of each structure (see **Supplementary Material A**. Volume and relative density computation). For the bounding box, the minimum rectangular solid that can contain the whole structure was considered.

The seven types of structures tested are shown in Fig. 4**.** They have been clustered into three groups, each sharing the same relative density. One structure has been taken as a reference for each group. They are always those with the twinned region because they are more complex to design and fabricate than the not twinned ones or the Octet. In addition, these structures are characterised by the same a and r values (Fig. 4). We decided to set these values a priori to keep under control their manufacturability. The relative density of these reference structures has been considered an input for the Matlab model to dimension the other structures. Different relative densities were inevitably obtained for the three groups. Additional details are provided in the Supplementary Material (see **Supplementary Material B**. Structures' details). As shown in Fig. 4, the Octet ("OT") structure was also included in the study, specifically in Group 1. Besides, it was decided to study: 1) the influence of the vertical extension (affecting the height "H" of the structure, Fig. 4) of the twinned region and 2) the influence of the extension of the non-twinned one on the mechanical behaviour of the structure. In this second case, the sample's length "L" (Fig. 4) changes. The resulting new variants are TwHCP_H and HCP_H in the first case and TwHCP_L and HCP_L in the second.

Table 1
Terminology and geometrical details of the seven samples analysed in this work (see also Fig. 4). The 7 structures are detailed in Supplementary Fig. B.1, B.2, and B.3.

Group	Name	Design category	Relative density [-]	a [mm]	r [mm]	Details
1st	*OT*	Octet	0.34	–	1	Sample sizes: 44.5x33.9x23.2 mm^3 (4x3x2 array, cell size 10.6 mm)
	HCP	Hexagonal close-packed		6.14	0.9	Sample sizes:44.9x33.8x22.5 mm^3 (7x3x2 array)
	TwHCP	Twinned HCP		6.00	0.9	Sample sizes: 43.8x34.7x22.5 mm^3 (3 repetitions of the "base" twinned unit cell performed along the y-direction)
2nd	*HCP_H*	Hexagonal close-packed	0.35	6.16	0.9	Sample sizes: 51.5x33.8x33 mm^3 (8x3x3 array)
	TwHCP_H	Twinned HCP		6.00	0.9	Sample sizes: 49.8x34.7x32.9 mm^3 (3 repetitions of the "base" twinned unit cell performed along the y direction, and 2 repetitions along the z-direction)
3rd	*HCP_L*	Hexagonal close-packed	0.37	6.16	0.9	Sample sizes: 69.6x33.8x22.6 mm^3 (11x3x2 array)
	TwHCP_L	Twinned HCP		6.00	0.9	Sample sizes: 67.8x34.7x22.6 mm^3 (3 repetitions of the "base" wider twinned unit cell performed along the y-direction)

The details of the samples are reported in Table 1 and in Supplementary Fig. B.1, B,2, and B.3. All the choices about beam radius and length, relative density, and array (Table 1) were motivated by the need to find a trade-off between the manufacturability of the structures and the requirement of equal relative density and overall volume.

Slight differences in the sample's overall dimensions, beam length and radius are inevitable to guarantee an equivalent relative density considering the different cell shapes. Concerning beams' length, the main difference concerns *a* and involves twinned HCP and HCP structures (i.e., 6.00 mm vs. 6.14 mm, respectively, Table 1). However, this difference is less than 3%. For manufacturability reasons, geometrical parameters (i.e., beam length *a* and radius *r*) were kept constant among structure categories: this implies a slight increase in the relative density of the variants compared to the structure of the first group. However, it is worth noting that direct comparisons were performed only among structures belonging to the same group and, therefore, among those having the same relative density.

3.2. Sample fabrication

All the structures were fabricated using Material Extrusion (MEX) and, specifically, a Fused Filament Fabrication (FFF) 3D printer (*Ultimaker 3*) with polylactic acid (PLA) filament with a diameter of 2.85 mm (*Ultimaker black PLA*). The standard extruder with a nozzle diameter equal to 0.4 mm was used. The mechanical properties of the material provided by the manufacturer can be found in [64].

The software *Ultimaker Cura v. 5.2.1* was used for the slicing; the default parameters of the "Normal – 0.15 mm profile" were selected, imposing an infill density equal to 100%. Three replicas were printed for each structure. Three additional TwHCP lattice samples were printed at a 0.10 mm layer height (instead of the standard 0.15 mm) to quantify this parameter's influence. Overall, 24 samples were printed and tested. Each sample was printed separately. Besides, all samples were weighed before testing using a precision digital weight scale (Kern PCB 2500–2, 0.01 g resolution). Pictures of the 3D-printed samples are reported in the Supplementary Material (see **Supplementary Material C**. 3D-printed samples).

3.3. Mechanical testing

Compressive tests were conducted under displacement control using an MTS Alliance RF/150 testing machine with a 150kN load cell at a strain rate of 0.003 s^{-1} (room temperature). The loading direction was consistent with the printing direction; the tests were terminated at a strain of 50%. The stress–strain nominal curves were extracted by dividing the recorded forces by the nominal cross-section area of the bounding box of the lattice to get the nominal stress and dividing the change in length along the applied displacement direction by the initial length to obtain the nominal strain. Elastic modulus and peak stress were extracted according to the slope of the first linear region and the highest recorded stress before plastic deformation, respectively. The specific energy absorption (SEA) and the densification strain were calculated according to the equations provided in [7,28,44,65–68]. Specifically, the SEA is defined as the energy absorption per unit mass, expressed as Eq. (1):

$$SEA = \frac{EA}{m} = \frac{1}{m}\int_0^d \frac{F(x)}{A}dx \tag{1}$$

where *EA* represents the energy-absorption capacity until densification *d*, *m* is the mass of the structure, $F(x)$ the force and A, the nominal area. Energy absorption per unit volume can also be quantified as the area under the stress–strain curve, as Eq. (2):

$$W_v = \int_0^{\varepsilon_d} \sigma d\varepsilon \tag{2}$$

where ε_d is the densification strain. This latter can be calculated by adopting an energy-absorption efficiency method, as explained in [44], defined as Eq. (3):

$$\varphi(\varepsilon) = \frac{\int_0^{\varepsilon}\sigma(\varepsilon)d\varepsilon}{\sigma(\varepsilon)} \tag{3}$$

with the densification strain defined as the strain at which $\varphi(\varepsilon)$ reaches its maximum value, satisfying Eq. (4):

$$\left.\frac{d\varphi(\varepsilon)}{d\varepsilon}\right|_{\varepsilon=\varepsilon_d} = 0 \tag{4}$$

Hardening rate ($\frac{d\sigma}{d\varepsilon}$) curves were plotted to quantify the stabilisation of the deformation behaviour. The compressive tests were filmed with a Nikon D7200 camera. Snapshots have been extracted from the video to analyse the compressive behaviour of the samples.

4. Results and discussion

Drawing inspiration from the remarkable compressive properties of ductile metals, the described approach investigates the innovative design of an HCP lattice structure crafted to emulate the crystal arrangement found in these metals. Leveraging the structural arrangement derived from the crystallographic characteristics of Ti and Zr, engineered metamaterials with unprecedented mechanical resilience were obtained. Central to the methodology is integrating the twinning phenomenon, a hallmark mechanism underlying the plastic deformation observed in these metals. By harnessing the intrinsic capability of twinning to redistribute stress, the deformation behaviour of the studied metamaterials was modified, boosting their structural integrity and significantly augmenting their energy absorption capacity.

Firstly, the correctness of the design procedure and the analytical

Table 2
Theoretical and experimental masses of the samples (see also Table 1). The $\Delta_{(th-exp)}$ [%] is calculated as: $(m_{th} - m_{exp})/m_{th}$*100.

Group		Theoretical [g]	Experimental ($\mu \pm \sigma$) [g]	$\Delta_{(th-exp)}$[%]
	TwHCP	14.7	14.45 ± 0.03	1.68
1st	*HCP*	14.7	14.47 ± 0.12	1.56
	OT	14.7	14.50 ± 0.06	1.34
	TwHCP_01	14.7	14.84 ± 0.02	−0.93
2nd	*TwHCP_L*	24.3	23.93 ± 0.07	1.54
	HCP_L	24.3	23.91 ± 0.01	1.60
3rd	*TwHCP_H*	24.9	23.08 ± 0.16	7.30
	HCP_H	24.9	24.28 ± 0.66	2.48

model implemented is discussed. Table 2 reports printed sample weights (mean ± standard deviation) and the theoretical values.

Each group's weights are comparable and exhibit low standard deviation, guaranteeing the repeatability of the manufacturing process. The comparability among samples within the same group demonstrates that the implemented design process has ensured the equivalence of volumes and, thus, weights for each group. Except for the three additional samples printed at 0.1 mm layer height (i.e., TwHCP_01 in Group 1), all samples are lighter than their theoretical weight, meaning that an under-extrusion of the material has occurred. Lowering the layer height has instead led to an over-extrusion. A maximum difference of 7.30% between the average weight and the theoretical value was measured for the *TwHCP_H* structure and, in general, for the second group of samples (Fig. 4 and Table 2) due to the increased complexity of the geometry to be printed compared to the others. Possible factors contributing to the differences between theoretical and experimental weight may be intrinsic porosity due to the AM process and approximations introduced by the slicing process. However, a good degree of repeatability can be observed within the same group of samples.

4.1. Compression test results

Fig. 5 reports mechanical tests of the designed crystal-inspired configurations, the stress–strain curves, and the deformation mechanisms of the three types of structures in Group 1 (Fig. 4).

The Octet structure (Fig. 5 a) exhibits the well-known stretching-dominated behaviour, with a softening after the peak stress. A layer-by-layer collapse characterises the deformation behaviour (see Snapshot IV of Fig. 5 a, where the white rectangle highlights the collapsed first layer). It does not present the shear-band formation typical of Octet structures [69]. This is due to a poor choice of the number of cell repetitions in the three directions, which is lower than the one suggested in the literature [17] for material homogenisation purposes. However, as explained in Section 3.1.3, this design choice was motivated by the need to design structures sharing an equivalent relative density compared to the reference structure.

The HCP (Fig. 5 b), as expected by its high connectivity, has a

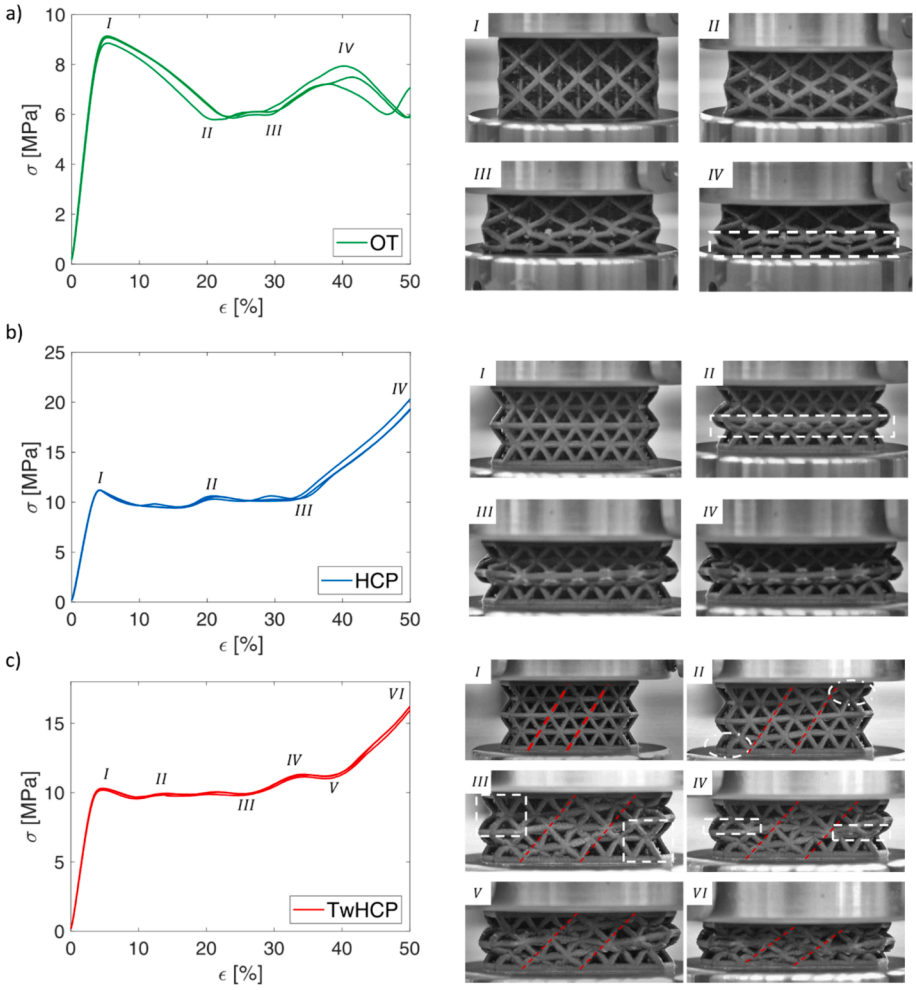

Fig. 5. Compressive stress–strain curves and deformation mechanism of the Octet (a), HCP (b) and TwHCP (c) structures (Group 1, Fig. 4). The red dotted lines in c represent the twin boundaries. For the y-axis, different scales were used to better highlight the fluctuations of the curves. Three samples were tested for each structure. (For interpretation of the references to colour in this figure legend, the reader is referred to the web version of this article.)

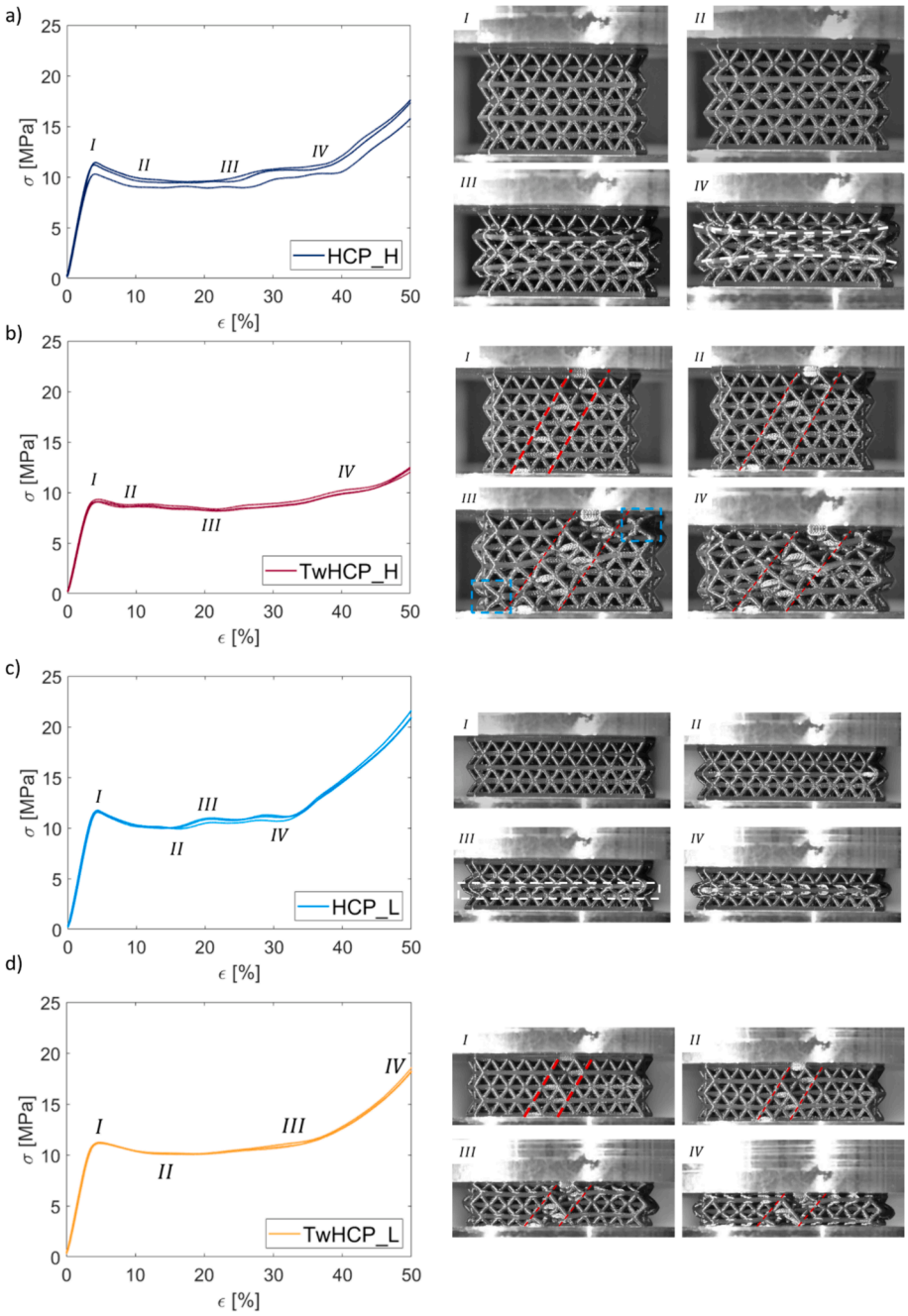

Fig. 6. Compressive stress–strain curves and deformation mechanism of the HCP_H (a), TwHCP_H (b), HCP_L (c), and TwHCP_L (d) structures. The red dotted lines in (b) and (d) represent the twin boundaries. Three samples were tested for each structure. (For interpretation of the references to colour in this figure legend, the reader is referred to the web version of this article.)

stretching-dominated behaviour too: compared to the Octet, the post-softening behaviour is slower, and the plastic plateau is broader and does not present wide fluctuations. Snapshots highlight how the deformation concentrates around the middle triangular layer (white dotted box in Snapshot II, Fig. 5 b), creating a shear band parallel to the compression plates. A small increase of the stress is reported around $\varepsilon = 20\%$ (Shapshot II, Fig. 5 b), with a consequent stabilisation. This can be explained by the collapse of a layer of vertical beams.

The TwHCP structure (Fig. 5 c), whose deformation behaviour is again one of stretching-dominated structures, is characterised by a minor stress reduction after the yielding (equal to −12.4 and −4.4% for the HCP and the TwHCP, respectively) and a wider and broader plateau with respect to the HCP structure. Interestingly, the deformation mode is changed by introducing the twin boundaries: the shear bands highlighted in the HCP structure do not extend horizontally throughout the whole sample. It can be noticed from the snapshots that the buckling of the struts starts in the region where the geometry is affected the most by the presence of the twinned area; at the outer boundaries, the lack of multiple HCP cells, which provide high stiffness, represents an initiation site for the plastic deformation of the structure (white dotted circles in Snapshot II, Fig. 5**c**). The deformation is then reported to proceed as a subsequent failure of HCP vertical strut layers. It is initiated in the areas featuring fewer HCPs in the x-direction and proceeds to the ones with a higher number of HCPs, thus leading to a "rotation" of the twinned area during the deformation. The farther regions from the twin boundaries are the last to deform (white dotted squares in Snapshot III, Fig. 5 c),

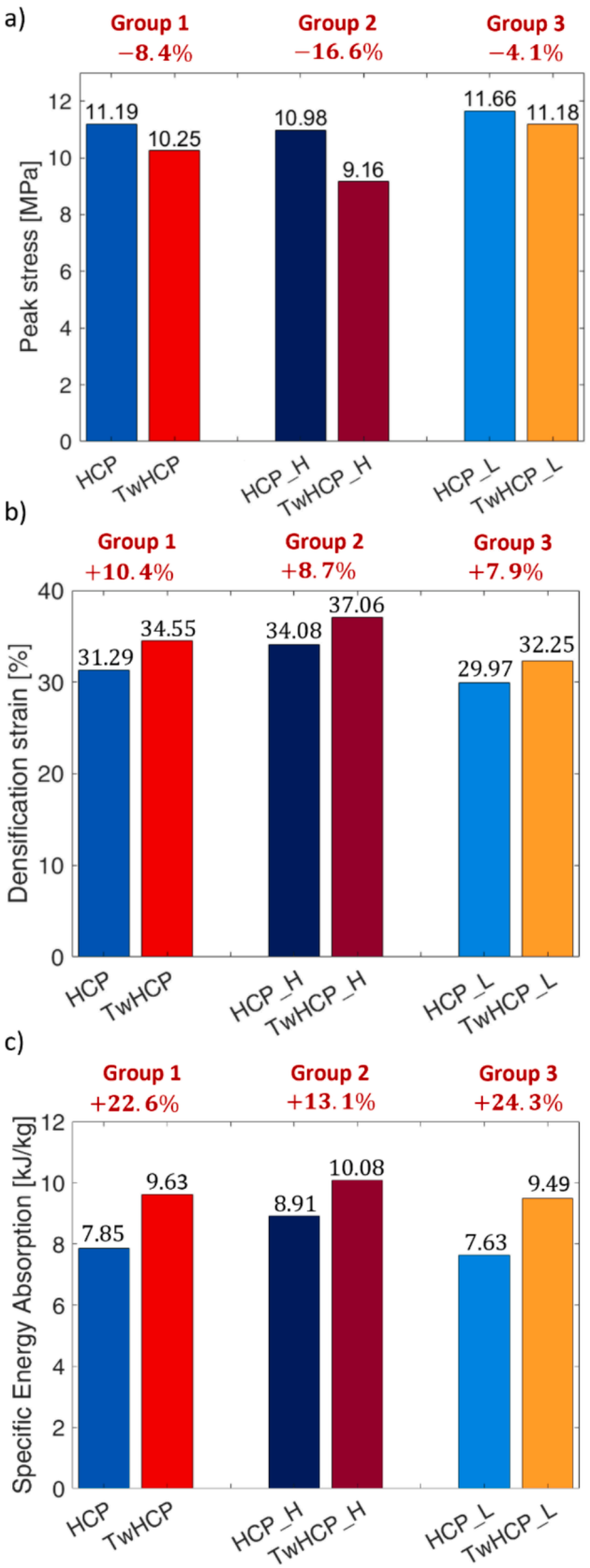

Fig. 7. Comparison between all the HCP and twinned HCP structures: histograms showing the peak stress decrease (a), the densification strain increase (b), and the specific energy absorption increase (c) induced by introducing a twinned area in an HCP lattice.

confirming that the introduction of the twinned region affects the deformation. The second stress plateau typical of HCP can be explained equivalently as the failure of the vertical beam layer highlighted by the white dotted boxes in Snapshot IV, Fig. 5 c. The behaviour of the TwHCP_01 samples (not reported in Fig. 5) is almost identical to that of the TwHCP ones, documenting a negligible influence of the layer height parameter. Further details are reported in the Supplementary Material (see **Supplementary Material** D. TwHCP_01).

To expand the comparison between the HCP and TwHCP and deepen the comprehension of the effects induced by the presence of the twinned region, the two variants TwHCP_H and TwHCP_L were introduced and tested along with their equivalent non-twinned structures HCP_H and HCP_L (Fig. 4, Group 2 and Group 3).

The HCP_H stress–strain curves are reported in Fig. 6 a. They show similar overall behaviour to the one observed from HCP, with softening after the stress peak and fluctuations due to layer-by-layer collapse. It is interesting to observe how multiple HCP layers induce curvature of the triangular grids in the central regions during the compression. The white dotted lines in Snapshot IV in Fig. 6 a highlight the curvature: this behaviour suggests that possible new deformation modes arise as the lattice dimension increases (HCP vs HCH_H) due to the homogenisation of the material. The TwHCP_H structure shows a more homogeneous deformation than the previously analysed TwHCP structure (Fig. 5 c). As shown in Fig. 6 b, the deformation is localised inside the twinned area. The first deformation in the HCP region occurs again in the outer boundaries next to the twin interface, as they are not part of a continuous lattice. These locations are highlighted by the light blue dotted squares in Snapshot III in Fig. 6 b.

The HCP_L stress–strain curves, shown in Fig. 6 c, confirm the stretching-dominated behaviour of the HCP cell, with shear bands formation along the central triangular layer. Eventually, the increase in the HCP region at the edges of a twinned lattice brought the desired results, as the stress–strain curves of the TwHCP_L lattice (Fig. 6 d) present almost no fluctuations. From the snapshots, it can be noticed that the formation of shear bands occurs in the HCP areas. Still, they are not allowed to propagate across the entire structure due to the discontinuity provided by the twinned region.

Pertaining the quantification of the twinning effect, Fig. 7 shows that all the samples featuring the twinned area present a decrease in the peak stress (ranging from −4.1 to −16.6%, Fig. 7 a), an extension of the plastic plateau, characterised by later densification (the increase of the densification strain ranges from 7.9 to 10.4%, Fig. 7 b) and an increase of the SEA with respect to the equivalent HCP structure (up to 24.3%, Fig. 7 c). Quantitative comparisons were performed on structures belonging to the same group, therefore sharing the same relative density. The comparisons of the stress–strain and hardening rate curves, those useful to visualise the stabilisation of the plastic deformation behaviour, are shown in Fig. 8 a and Fig. 8 b, respectively. These findings are aligned with the ones found by other authors in the literature [28,42–44] because the energy absorption is increased without negatively affecting the peak stress. In addition, our study rigorously proves the effectiveness of mimicking the atomic phenomenon at higher scales. The greatest enhancement in the specific energy absorption was experienced by the TwHCP_L, featuring a larger amount of HCP lattice on the sides of the twinned area. In such a structure, the interruption of the shear bands due to the twinning boundaries prevents the layer-by-layer collapse, limiting the stress fluctuations in the post-yielding phase.

Hence, the emulation of metallographic phenomena, particularly the incorporation of the twinning mechanism into the HCP lattice, has demonstrated significant efficacy in altering the deformation characteristics of materials. This alteration results in heightened energy absorption capabilities, showcasing a promising avenue for material engineering and design. By integrating twinning mechanisms into the lattice structure, researchers have been able to enhance the material's ability to absorb energy, which has numerous positive implications across various application fields. Specifically, this study opens up new

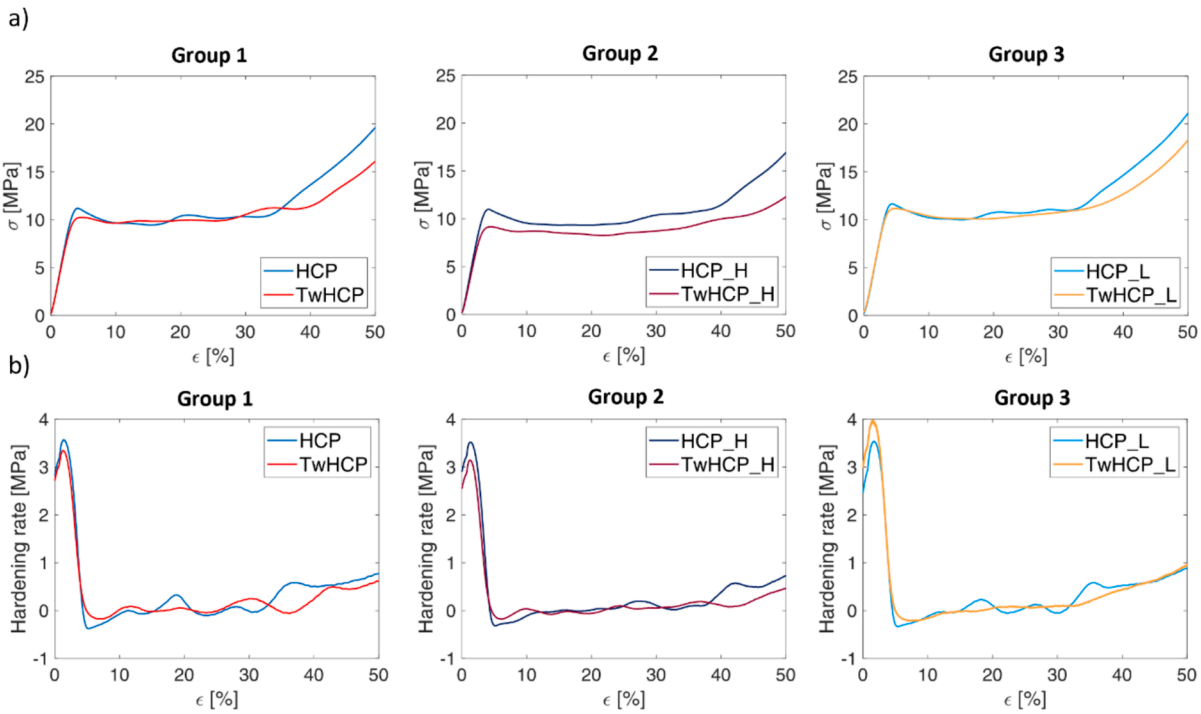

Fig. 8. Comparison between all the HCP and twinned HCP structures (Fig. 4): stress–strain (a) and hardening rate (b) curves of the three couples of HCP and twinned HCP analysed in this study. Mean curves are reported for each structure; shaded error bars are not reported due to the high superimposition of the curves (see also Fig. 5 and Fig. 6).

possibilities for advancing the design of architected materials, particularly in areas where energy absorption is crucial, such as aerospace [70,71], wearable technology and biomedicine [72,73], and construction [74]. In aerospace, materials with enhanced energy absorption capabilities can be employed to guarantee the safety of passengers and equipment, mitigating the damage caused by collisions or crashes, potentially saving lives, and reducing maintenance and repair costs. Energy absorption is also essential for enhancing comfort, safety, and effectiveness concerning wearables and biomedicine. Finally, in the construction industry, materials with enhanced energy absorption capabilities can enhance the resilience of structures against natural disasters, such as earthquakes or heavy machinery's impacts.

To further explore the potential of this approach, different AM technologies and materials can be investigated for sample fabrication, depending on the specific application field. Once the appropriate material is selected for the targeted application, the design and number of twinned regions can be fine-tuned to ensure the desired behaviour in terms of peak stress and plastic plateau. Moreover, the implementation of twinning regions, including the selection of the twinning plane used to design them, can be adjusted according to the specific loading conditions under analysis. This flexibility allows the tailoring of the material properties to meet the requirements of various real-world scenarios, maximising its effectiveness in practical applications.

5. Conclusions

This study is inspired by the compressive behaviour of ductile metals with a hexagonal close-packed structure experiencing the metallurgical twinning phenomenon. It proposes a novel architected material based on an HCP unit cell and a modification of the same by introducing this twinning phenomenon at higher scales. As for Ti and Zr ductile metals, the twinning mechanism accommodates the compressive load by plastic deformation. Introducing a twinned zone inside a homogenous HCP lattice stabilises the deformation behaviour and increases the energy absorption capabilities up to 24.3% without compromising mechanical properties excessively. In this study, the HCP lattice was studied, but the proposed approach could be extended to other unit cells, such as the BCC unit cell, because it is often considered for energy-absorbing applications in combination with materials such as TPU [75]. The BCC has a lower packing density than FCC and HCP; thus, it is less prone to slip deformation mechanisms, and has several twinning mechanisms that could be reproduced by adopting the same design approach described in the paper. This study could be extended by considering other twinning planes based on the loading conditions. In addition, it could be interesting to repeat the study considering the ductile metals used as inspiration as the base material. One limitation of the study resides in the necessity for extensive manual adjustments in generating the digital model of the twinned structure, particularly concerning guaranteeing node connectivity. In the future, implementing more automated procedures could streamline the generation of these twinned regions, enhancing efficiency and accuracy in modelling.

CRediT authorship contribution statement

Giovanni Zappa: Writing – review & editing, Writing – original draft, Visualization, Validation, Software, Methodology, Investigation, Formal analysis, Data curation, Conceptualization. **Lorenzo Cocchi:** Writing – review & editing, Writing – original draft, Software, Methodology, Conceptualization. **Sara Candidori:** Writing – review & editing, Writing – original draft, Visualization, Validation, Supervision, Methodology, Investigation, Formal analysis, Data curation, Conceptualization. **Federica Buccino:** Writing – review & editing, Writing – original draft, Visualization, Validation, Supervision, Methodology, Investigation, Formal analysis, Data curation, Conceptualization. **Laura Vergani:** Writing – review & editing, Writing – original draft, Supervision, Resources, Project administration, Methodology, Conceptualization. **Serena Graziosi:** Writing – review & editing, Writing – original draft, Supervision, Resources, Methodology, Conceptualization.

Declaration of competing interest

The authors declare that they have no known competing financial interests or personal relationships that could have appeared to influence the work reported in this paper.

Data availability

The data that support the findings of this study are available from the corresponding author upon reasonable request.

Acknowledgement

The authors wish to thank the students Francesco Carrozza, Nicoletta Gemello, Emmanuel Denis Manoni, Giacomo Scagnetti and Filippo Zoia of the School of Industrial and Information Engineering of Politecnico di Milano for their technical support in the preliminary stages of this research. This study was carried out within the MICS (Made in Italy - Circular and Sustainable) Extended Partnership and received funding from the European Union Next-GenerationEU (PIANO NAZIONALE DI RIPRESA E RESILIENZA (PNRR) - MISSIONE 4 COMPONENTE 2, INVESTIMENTO 1.3 - D.D. 1551.11-10-2022, PE00000004). This manuscript reflects only the authors' views and opinions, neither the European Union nor the European Commission can be considered responsible for them.

Appendix A. Supplementary data

Supplementary data to this article can be found online at https://doi.org/10.1016/j.matdes.2024.113098.

References

[1] P. Jiao, J. Mueller, J.R. Raney, X. Zheng, A.H. Alavi, Mechanical metamaterials and beyond, Nat. Commun. 14 (2023) 6004, https://doi.org/10.1038/s41467-023-41679-8.
[2] A.A. Zadpoor, Mechanical meta-materials, Mater. Horizons. 3 (2016) 371–381, https://doi.org/10.1039/c6mh00065g.
[3] F. Buccino, P. Bruzzaniti, S. Candidori, S. Graziosi, L. Maria Vergani, Tailored torsion and bending-resistant avian-inspired structures, Adv. Eng. Mater. 2200568 (2022) 1–9. https://doi.org/10.1002/adem.202200568.
[4] M.F. Ashby, The properties of foams and lattices, Philos. Trans. R. Soc. A Math. Phys, Eng. Sci. 364 (2006) 15–30, https://doi.org/10.1098/rsta.2005.1678.
[5] L.J. Gibson, M.F. Ashby, Cellular solids - Structure and properties, 2nd editio, Press Syndicate of the University of Cambridge, Cambridge, 1997.
[6] F. Tamburrino, S. Graziosi, M. Bordegoni, The design process of additively manufactured mesoscale lattice structures: A review, J. Comput. Inf. Sci. Eng. 18 (2018) 1–16, https://doi.org/10.1115/1.4040131.
[7] T. Tancogne-Dejean, A.B. Spierings, D. Mohr, Additively-manufactured metallic micro-lattice materials for high specific energy absorption under static and dynamic loading, Acta Mater. 116 (2016) 14–28, https://doi.org/10.1016/j.actamat.2016.05.054.
[8] V.S. Deshpande, M.F. Ashby, N.A. Fleck, Foam topology: bending versus stretching dominated architectures, Acta Mater. 49 (2001) 1035–1040, https://doi.org/10.1016/S1359-6454(00)00379-7.
[9] J. Bauer, L.R. Meza, T.A. Schaedler, R. Schwaiger, X. Zheng, L. Valdevit, Nanolattices: An Emerging Class of Mechanical Metamaterials, Adv. Mater. 29 (2017) 1–26, https://doi.org/10.1002/adma.201701850.
[10] M. Leary, M. Mazur, H. Williams, E. Yang, A. Alghamdi, B. Lozanovski, X. Zhang, D. Shidid, L. Farahbod-Sternahl, G. Witt, I. Kelbassa, P. Choong, M. Qian, M. Brandt, Inconel 625 lattice structures manufactured by selective laser melting (SLM): Mechanical properties, deformation and failure modes, Mater. Des. 157 (2018) 179–199, https://doi.org/10.1016/j.matdes.2018.06.010.
[11] Z. Vangelatos, K. Komvopoulos, C.P. Grigoropoulos, Regulating the mechanical behavior of metamaterial microlattices by tactical structure modification, J. Mech. Phys. Solids. 144 (2020) 104112, https://doi.org/10.1016/j.jmps.2020.104112.
[12] R. Gümrük, R.A.W. Mines, Compressive behaviour of stainless steel micro-lattice structures, Int. J. Mech. Sci. 68 (2013) 125–139, https://doi.org/10.1016/j.ijmecsci.2013.01.006.
[13] D. Qi, H. Yu, M. Liu, H. Huang, S. Xu, Y. Xia, G. Qian, W. Wu, Mechanical behaviors of SLM additive manufactured octet-truss and truncated-octahedron lattice structures with uniform and taper beams, Int. J. Mech. Sci. 163 (2019) 105091, https://doi.org/10.1016/j.ijmecsci.2019.105091.
[14] H.Z. Zhong, T. Song, C.W. Li, R. Das, J.F. Gu, M. Qian, Understanding the superior mechanical properties of hollow-strut metal lattice materials, Scr. Mater. 228 (2023) 2–7, https://doi.org/10.1016/j.scriptamat.2023.115341.
[15] Y. Huang, Y. Xue, X. Wang, F. Han, Effect of cross sectional shape of struts on the mechanical properties of aluminum based pyramidal lattice structures, Mater. Lett. 202 (2017) 55–58, https://doi.org/10.1016/j.matlet.2017.05.073.
[16] M.Q. Shaikh, S. Graziosi, S.V. Atre, Supportless printing of lattice structures by metal fused filament fabrication (MF3) of Ti-6Al-4V: design and analysis, Rapid Prototyp. J. 27 (2021) 1408–1422, https://doi.org/10.1108/RPJ-01-2021-0015.
[17] I. Maskery, L. Sturm, A.O. Aremu, A. Panesar, C.B. Williams, C.J. Tuck, R. D. Wildman, I.A. Ashcroft, R.J.M. Hague, Insights into the mechanical properties of several triply periodic minimal surface lattice structures made by polymer additive manufacturing, Polymer (guildf). 152 (2018) 62–71, https://doi.org/10.1016/j.polymer.2017.11.049.
[18] E. Chen, S. Luan, S. Gaitanaros, On the compressive strength of brittle lattice metamaterials, Int. J. Solids Struct. 257 (2022) 111871, https://doi.org/10.1016/j.ijsolstr.2022.111871.
[19] Y. Jiang, Q. Wang, Highly-stretchable 3D-architected Mechanical Metamaterials, Sci. Rep. 6 (2016) 1–11, https://doi.org/10.1038/srep34147.
[20] M.S. Pham, C. Liu, I. Todd, J. Lertthanasarn, Damage-tolerant architected materials inspired by crystal microstructure, Nature. 565 (2019) 305–311, https://doi.org/10.1038/s41586-018-0850-3.
[21] T. Maconachie, M. Leary, B. Lozanovski, X. Zhang, M. Qian, O. Faruque, M. Brandt, SLM lattice structures: Properties, performance, applications and challenges, Mater. Des. 183 (2019) 108137, https://doi.org/10.1016/j.matdes.2019.108137.
[22] L. Liu, P. Kamm, F. García-Moreno, J. Banhart, D. Pasini, Elastic and failure response of imperfect three-dimensional metallic lattices: the role of geometric defects induced by Selective Laser Melting, J. Mech. Phys. Solids. 107 (2017) 160–184, https://doi.org/10.1016/j.jmps.2017.07.003.
[23] I. Echeta, X. Feng, B. Dutton, R. Leach, S. Piano, Review of defects in lattice structures manufactured by powder bed fusion, Int. J. Adv. Manuf. Technol. 106 (2020) 2649–2668, https://doi.org/10.1007/s00170-019-04753-4.
[24] F. Han, B. Lattice, in: Probl., Solid State Phys. with Solut, World Scientific (2011) 29–41, https://doi.org/10.1142/9789814365031_0003.
[25] T.S. Lumpe, T. Stankovic, Exploring the property space of periodic cellular structures based on crystal networks, Proc. Natl. Acad. Sci. U. S. A. 118 (2021), https://doi.org/10.1073/pnas.2003504118.
[26] A. Leuenberger, E. Birner, T.S. Lumpe, T. Stankovic, Computational Design of 2D Lattice Structures based on Crystallographic Symmetries, J. Mech. Des. 146 (2023) 1–30, https://doi.org/10.1115/1.4064246.
[27] F. Libonati, S. Graziosi, F. Ballo, M. Mognato, G. Sala, 3D-Printed Architected Materials Inspired by Cubic Bravais Lattices, ACS Biomater. Sci. Eng. (2021), https://doi.org/10.1021/acsbiomaterials.0c01708.
[28] Y. Bian, F. Yang, P. Li, P. Wang, W. Li, H. Fan, Energy absorption properties of macro triclinic lattice structures with twin boundaries inspired by microstructure of feldspar twinning crystals, Compos. Struct. 271 (2021), https://doi.org/10.1016/j.compstruct.2021.114103.
[29] C. Liu, J. Lertthanasarn, M.S. Pham, The origin of the boundary strengthening in polycrystal-inspired architected materials, Nat. Commun. 12 (2021) 1–10, https://doi.org/10.1038/s41467-021-24886-z.
[30] E.O. Hall, The deformation and ageing of mild steel: III Discussion of results, Proc. Phys. Soc. Sect. B. 64 (1951) 747–753, https://doi.org/10.1088/0370-1301/64/9/303.
[31] N.J. Petch, The cleavage strength of polycrystals, J. Iron Steel Inst. 174 (1953) 25–28.
[32] J. Lertthanasarn, C. Liu, M.S. Pham, Synergistic effects of crystalline microstructure, architected mesostructure, and processing defects on the mechanical behaviour of Ti6Al4V meta-crystals, Mater. Sci. Eng. A. 818 (2021) 141436, https://doi.org/10.1016/j.msea.2021.141436.
[33] D.G. Brandon, The structure of high-angle grain boundaries, Acta Metall. 14 (1966) 1479–1484, https://doi.org/10.1016/0001-6160(66)90168-4.
[34] J. Yang, X. Chen, Y. Sun, C. Feng, Z. Yang, A.A. Zadpoor, M.J. Mirzaali, L. Bai, Rational design and additive manufacturing of grain boundary-inspired, multi-architecture lattice structures, Mater. Des. 235 (2023) 112448, https://doi.org/10.1016/j.matdes.2023.112448.
[35] C. Liu, M. Pham, Spatially Programmable Architected Materials Inspired by The Metallurgical Phase Engineering, Adv. Mater. (2023), https://doi.org/10.1002/adma.202305846.
[36] A.J. Ardell, Precipitation hardening, Metall. Trans. A. 16 (1985) 2131–2165.
[37] T. Gladman, Precipitation hardening in metals, Mater. Sci. Technol. 15 (1999) 30–36, https://doi.org/10.1179/026708399773002782.
[38] R.W. Cahn, P. Haasen, Physical metallurgy, Elsevier, Fourth, 1996.
[39] J. Lertthanasarn, C. Liu, M.-S. Pham, Influence of the base material on the mechanical behaviors of polycrystal-like meta-crystals, J. Micromechanics Mol. Phys. 06 (2021), https://doi.org/10.1142/S2424913021500041.
[40] M.A. Saccone, R.A. Gallivan, K. Narita, D.W. Yee, J.R. Greer, Additive manufacturing of micro-architected metals via hydrogel infusion, Nature. 612 (2022) 685–690, https://doi.org/10.1038/s41586-022-05433-2.
[41] K. Lu, L. Lu, S. Suresh, Strengthening materials by engineering coherent internal boundaries at the nanoscale, Science (80-.). 324 (2009) 349–352, https://doi.org/10.1126/science.1159610.
[42] K. Song, D. Li, T. Liu, C. Zhang, Y. Min Xie, W. Liao, Crystal-twinning inspired lattice metamaterial for high stiffness, strength, and toughness, Mater. Des. 221 (2022) 1–18, https://doi.org/10.1016/j.matdes.2022.110916.
[43] Y. Zhang, J. Zhang, X. Zhao, Y. Li, S. Che, W. Yang, L. Han, Mechanical behaviors regulation of triply periodic minimal surface structures with crystal twinning, Addit. Manuf. 58 (2022) 103036, https://doi.org/10.1016/j.addma.2022.103036.

[44] W. Wu, S. Kim, A. Ramazani, Y. Tae Cho, Twin mechanical metamaterials inspired by nano-twin metals: Experimental investigations, Compos. Struct. 291 (2022) 115580, https://doi.org/10.1016/j.compstruct.2022.115580.
[45] E. Tenckhoff, Deformation Mechanisms, Texture, and Anisotropy in Zirconium and Zircaloy, ASTM International, 100 Barr Harbor Drive, PO Box C700, West Conshohocken, PA 19428-2959, 1988. https://doi.org/10.1520/STP966-EB.
[46] M.H. Yoo, Slip, twinning, and fracture in hexagonal close-packed metals, Metall. Trans. A. 12 (1981) 409–418, https://doi.org/10.1007/BF02648537.
[47] H. Gu, A. Shterenlikht, M. Pavier, Brittle fracture of three-dimensional lattice structure, Eng. Fract. Mech. 219 (2019) 106598, https://doi.org/10.1016/j.engfracmech.2019.106598.
[48] Y. Li, H. Gu, M. Pavier, H. Coules, Compressive behaviours of octet-truss lattices, Proc. Inst. Mech. Eng. Part C J. Mech. Eng. Sci. 234 (2020) 3257–3269, https://doi.org/10.1177/0954406220913586.
[49] Y. Li, M. Pavier, H. Coules, Fracture behaviour of octet-truss lattices in different orientations, Procedia Struct. Integr. 37 (2021) 49–56, https://doi.org/10.1016/j.prostr.2022.01.058.
[50] Y. Li, M. Pavier, H. Coules, Compressive fatigue characteristics of octet-truss lattices in different orientations, Mech. Adv. Mater. Struct. 29 (2022) 6390–6402, https://doi.org/10.1080/15376494.2021.1978020.
[51] Y. Li, M. Pavier, H. Coules, Experimental study on fatigue crack propagation of octet-truss lattice, Procedia Struct. Integr. 37 (2021) 41–48, https://doi.org/10.1016/j.prostr.2022.01.057.
[52] Y. Li, M. Pavier, H. Coules, Fatigue crack propagation of differently oriented octet-truss lattices, Int. J. Fatigue. 166 (2023) 107250, https://doi.org/10.1016/j.ijfatigue.2022.107250.
[53] Y. Li, M.M. Attallah, H. Coules, R. Martinez, M. Pavier, Fatigue of octet-truss lattices manufactured by Laser Powder Bed Fusion, Int. J. Fatigue. 170 (2023) 107524, https://doi.org/10.1016/j.ijfatigue.2023.107524.
[54] B.D. Cullity, Elements of X-Ray Diffraction, 2nd ed.,, Addison-Wesley Publishing, 1978.
[55] V.S. Deshpande, N.A. Fleck, M.F. Ashby, Effective properties of the octet-truss lattice material, J. Mech. Phys. Solids. 49 (2001) 1747–1769, https://doi.org/10.1016/S0022-5096(01)00010-2.
[56] C. Bonatti, D. Mohr, Smooth-shell metamaterials of cubic symmetry: Anisotropic elasticity, yield strength and specific energy absorption, Acta Mater. 164 (2019) 301–321, https://doi.org/10.1016/j.actamat.2018.10.034.
[57] J. Mueller, K.H. Matlack, K. Shea, C. Daraio, Energy Absorption Properties of Periodic and Stochastic 3D Lattice Materials, Adv. Theory Simulations. 2 (2019) 1–11, https://doi.org/10.1002/adts.201900081.
[58] W.O. Soboyejo, Crystal Structure and Dislocation Motion, in: Mech. Prop. Eng. Mater., 2ed ed., CRC Press, 2003.
[59] N. Munroe, X. Tan, H. Gu, Orientation dependence of slip and twinning in HCP metals, Scr. Mater. 36 (1997) 1383–1386, https://doi.org/10.1016/S1359-6462(97)00048-1.
[60] H. Fan, J.A. El-Awady, Molecular Dynamics Simulations of Orientation Effects during Tension, Compression, and Bending Deformations of Magnesium Nanocrystals, J. Appl. Mech. Trans. ASME. 82 (2015) 1–11, https://doi.org/10.1115/1.4030930.
[61] J.C. Williams, R.G. Baggerly, N.E. Paton, Deformation behavior of HCP Ti-Al alloy single crystals, Metall. Mater. Trans. A Phys. Metall. Mater. Sci. 33 (2002) 837–850, https://doi.org/10.1007/s11661-002-0153-y.
[62] E.C. Burke, W.R. Hibbard, Plastic Deformation of Magnesium Single Crystals, Jom. 4 (1952) 295–303, https://doi.org/10.1007/bf03397694.
[63] Food4Rhino, Intralattice, (n.d.). https://www.food4rhino.com/en/app/intralattice (accessed November 5, 2023).
[64] Ultimaker, Ultimaker PLA technical datasheet, (n.d.). https://makerbot.my.salesforce.com/sfc/p/#j0000000HOnW/a/5b000004UiRV/lt4XCkl0KOSLfPMcyG06mKKbES33WnYiFrMsG8bFGhw (accessed June 16, 2023).
[65] Z. Jia, F. Liu, X. Jiang, L. Wang, Engineering lattice metamaterials for extreme property, programmability, and multifunctionality, J. Appl. Phys. 127 (2020), https://doi.org/10.1063/5.0004724.
[66] P.J. Tan, J.J. Harrigan, S.R. Reid, Inertia effects in uniaxial dynamic compression of a closed cell aluminium alloy foam, Mater. Sci. Technol. 18 (2002) 480–488, https://doi.org/10.1179/026708302225002092.
[67] G. Belingardi, R. Montanini, M. Avalle, Characterization of polymeric structural foams under compressive impact loading by means of energy-absorption diagram, Int. J. Impact Eng. 25 (2001) 455–472.
[68] Z.P. Sun, Y.B. Guo, V.P.W. Shim, Characterisation and modeling of additively-manufactured polymeric hybrid lattice structures for energy absorption, Int. J. Mech. Sci. 191 (2021) 106101, https://doi.org/10.1016/j.ijmecsci.2020.106101.
[69] M. Kaur, T.G. Yun, S.M. Han, E.L. Thomas, W.S. Kim, 3D printed stretching-dominated micro-trusses, Mater. Des. 134 (2017) 272–280, https://doi.org/10.1016/j.matdes.2017.08.061.
[70] Y. Guo, J. Zhang, L. Chen, B. Du, H. Liu, L. Chen, W. Li, Y. Liu, Deformation behaviors and energy absorption of auxetic lattice cylindrical structures under axial crushing load, Aerosp. Sci. Technol. 98 (2020) 105662, https://doi.org/10.1016/j.ast.2019.105662.
[71] L. Li, F. Yang, P. Li, W. Wu, L. Wang, A novel hybrid lattice design of nested cell topology with enhanced energy absorption capability, Aerosp. Sci. Technol. 128 (2022) 107776, https://doi.org/10.1016/j.ast.2022.107776.
[72] S.F. Khosroshahi, S.A. Tsampas, U. Galvanetto, Feasibility study on the use of a hierarchical lattice architecture for helmet liners, Mater. Today Commun. 14 (2018) 312–323, https://doi.org/10.1016/j.mtcomm.2018.02.002.
[73] A.M. Vilardell, A. Takezawa, A. du Plessis, N. Takata, P. Krakhmalev, M. Kobashi, I. Yadroitsava, I. Yadroitsev, Topology optimization and characterization of Ti6Al4V ELI cellular lattice structures by laser powder bed fusion for biomedical applications, Mater. Sci. Eng. A. 766 (2019) 138330, https://doi.org/10.1016/j.msea.2019.138330.
[74] L. Traseira-Piñeiro, M. Bodaghi, A. Grizi, A. Garcia-Hernandez, G. Albertini, Energy-absorbing particles for enhanced mechanical performance of asphalt's aggregate skeleton, Constr. Build. Mater. 415 (2024) 135055, https://doi.org/10.1016/j.conbuildmat.2024.135055.
[75] S. Graziosi, F.M. Ballo, F. Libonati, S. Senna, 3D printing of bending-dominated soft lattices: numerical and experimental assessment, Rapid Prototyp. J. 28 (2022) 51–64, https://doi.org/10.1108/RPJ-03-2022-0095.